PIER C

Multi-Objective Optimization Design of Low-Torque Ripple Ferrite-Assisted Synchronous Reluctance Motor

Chaozhi Huang, Haiwen Li*, Siying Li, and Yanwen Sun

School of Electrical Engineering and Automation
Jiangxi University of Science and Technology, Ganzhou 341000, Jiangxi, China

ABSTRACT: In order to achieve the optimization objectives of low torque ripple, high torque, and high efficiency, this paper proposes a multi-objective optimization strategy based on genetic algorithms optimizing BP neural network (GA-BP) combined with non-dominated sorting genetic algorithm (NSGA-II) and applies it to the multi-objective optimization design of an external rotor ferrite-assisted synchronous reluctance motor (ERFa-SynRM). Firstly, the preliminary design and selection of ERFa-SynRM structure are carried out. Secondly, a comprehensive sensitivity analysis is presented on the extent to which the design variables affect the optimization objectives. Thirdly, a high-precision prediction model is constructed by GA-BP neural network, and NSGA-II is applied to global optimization of the prediction model. Finally, the electromagnetic performances of the motor before and after the optimization are compared by the finite element analysis (FEA) software. Compared with the initial motor, the average torque and efficiency of the optimized motor are improved, and the torque ripple is reduced by 54.9%, which verifies the effectiveness of the multi-objective optimization design method.

1. INTRODUCTION

In recent years, rare-earth permanent magnet (PM) materials have been extremely mined in various industries, and their prices have continued to rise, which have caused widespread concern in society. This trend of mass mining has intensified the dependence on rare earth PM materials and increased the risk of environmental damage. People have begun to actively explore alternatives to rare earth PM materials. Permanent magnet-assisted synchronous reluctance motor (PMaSynRM) stands out among many categories with its advantages of high performance, low cost, and energy saving. Nowadays, it has been widely utilized in electric vehicles, air conditioners, and washing machines [1, 2]. The PMaSynRM combines the advantages of SynRM and PMSM which has the advantages of wide speed regulation range, high power density, high efficiency, and light weight [3–5]. But it also has problems such as low power factor and high torque ripple, which restrict the development of PMa-SynRM.

The torque ripple of the PMa-SynRM mainly derives from the geometry structure of doubly salient electro-magnetic motor, which consists of a combination of cogging torque ripple, PM torque ripple, and reluctance torque ripple. The methods to reduce torque ripple can be generally divided into two types: changing the shape of the motor structure and optimizing the parameters of the motor structure. From the perspective of the motor structure shape, the influence of the SynRM adjacent flux barrier width ratio on the torque ripple is investigated, and a rotor topology with a gradual change of the flux barrier is proposed, which effectively suppresses the torque ripple of the motor [6]. In [7], a star rotor structure is proposed, which

increases the angle between the end of the rotor air-gap flux barrier and the q-axis, changes the distribution of the air-gap flux density, and effectively reduces the torque ripple and increases the output torque of the motor. In [8], the rotor structure with a W-notch for reducing the torque ripple is proposed, which increases the torque density of the external rotor PMaSynRM.

From the perspective of the optimization method, the design parameter values of the motor are determined by the optimization algorithm, which can effectively suppress the torque ripple and improve the average torque and operating efficiency of the motor. A new 10-pole, 48-slot external rotor Fa-SynRM topology is proposed, which is optimized for a multi-objective design using genetic algorithm (GA) and FEA model to achieve the design objectives of high efficiency and wide constant power speed ratio of the motor [9]. In [10], an optimal design method for a high-density external rotor PMa-SynRM for hub motors is presented, which is verified to have superior electromagnetic performance compared to an inner rotor motor of the same size by using the equivalent magnetic circuit and differential evolutionary (DE) algorithm. In [11], a method combining NSGA-II and FEA models is proposed to obtain a three-phase transformer with high efficiency, minimum losses, and low cost. An optimization strategy based on response surface model and improved multi-objective particle swarm optimization algorithm applied to a bearingless permanent magnet synchronous motor is investigated to increase the average suspension force and decrease the suspension force ripple [12]. In [13], a multi-objective design algorithm of GA-SVM combined with NSGA-II is proposed, so as to optimize the structure parameters of the motor for reducing the torque ripple. In [14], an optimal design method combining random forest technique

---

* Corresponding author: Haiwen Li (1751640057@qq.com).

and GA for the motor is presented, by which the performance of the motor is improved.

This paper proposes the multi-objective optimization design method based on GA-BP combined with NSGA-II. Firstly, the initial model of ERFa-SynRM is established. Secondly, the comprehensive sensitivity analysis of the influence of design variables on the electromagnetic performance of the motor is put forward to stratify the strong and weak sensitivities of more design variables of the motor. Then, the high-precision prediction model of the motor is built by GA-BP algorithm. Finally, NSGA-II is used to globally optimize the prediction model for obtaining the optimal motor structure.

2. DESIGN OF MOTOR STRUCTURE

ERFa-SynRM is driven by both reluctance torque and PM torque. Compared with IPMSM, the reluctance torque of ERFa-SynRM accounts for a larger proportion and requires less PM materials. The reasonable motor structure can overcome the problems of low torque density, high torque ripple, and low efficiency based on the optimization objectives and constraints of motor design. The initial design scheme of ERFa-SynRM is given in this section, considering the electromagnetic performance of the topology under various conditions. The rated power and speed of the initial model are 265 W and 350 r/min, respectively. A comparison of the average torque and torque ripple performance of the motor with or without PMs and different flux barrier layers is given in Table 1.

TABLE 1. Simulation results of average torque and torque ripple for different topologies.

Number of PMs	Two Flux Barriers $[T_{avg}, T_{rip}]$	Three Flux Barriers $[T_{avg}, T_{rip}]$
0	$[4.4\,\mathrm{N\cdot m}, 34.7\%]$	$[4.7\,\mathrm{N\cdot m}, 20.2\%]$
1PM	–	$[5.5\,\mathrm{N\cdot m}, 29.6\%]$
2PMs	–	$[6.4\,\mathrm{N\cdot m}, 26.8\%]$
3PMs	–	$[7.14\,\mathrm{N\cdot m}, 19\%]$

It can be seen from Table 1 that the number of rotor flux barriers directly affects the motor performance. With more layers of the flux barriers, the average torque increases, and the torque ripple decreases. The number of the rotor flux barriers is generally set to 2, 3 and 4. But the torque is almost unchanged with the increase of the number of layers of the flux barrier when the designed number of layers is greater than or equal to 4 [15]. Fig. 1 shows the simulation results of the average torque of two-layer and three-layer flux barriers with the same size and working conditions. It can be seen from Fig. 1 that the average torque and torque ripple of the two-layer flux barrier are 4.4 N·m and 34.7%, respectively, while those of the three-layer flux barrier are 4.7 N·m and 20.2%, respectively. The average torque performance of the motor increases, and the torque ripple performance decreases significantly with the increase of the number of layers of the flux barrier. Considering the constraints of mechanical stresses in the motor, three layers of the flux barrier are chosen to design the external rotor structure of ERFa-SynRM in this paper.
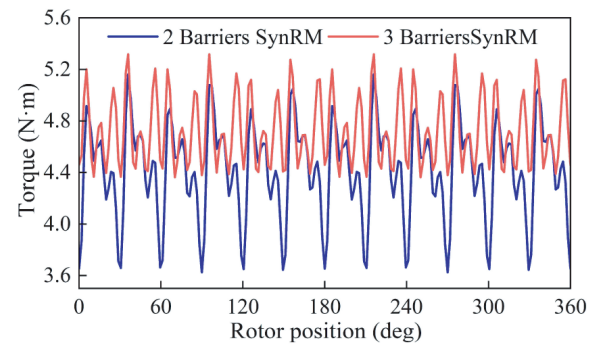
FIGURE 1. Average torque for different number of the flux barrier.
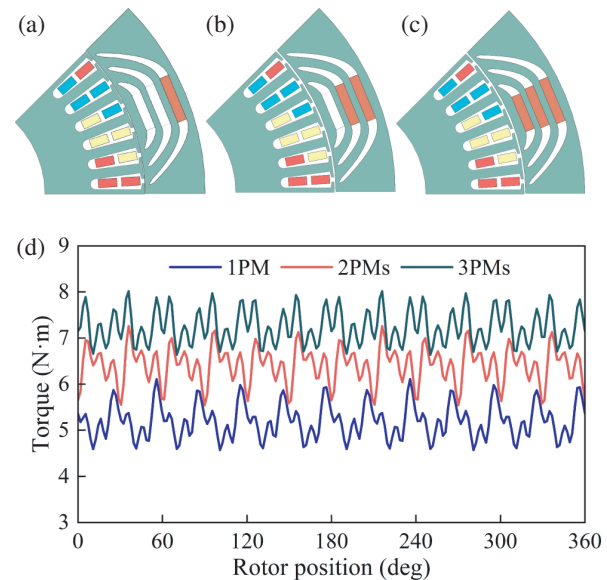
FIGURE 2. Rotor structure and simulation results for different number of PMs. (a) 1PM (b) 2PMs (c) 3PMs (d) Simulation results.

Furthermore, embedding PM materials in the flux barrier is also one of the factors to improve the performance of the motor. To find the optimal number of flux barriers, ferrite material is added to flux barrier of one layer, two layers, and three layers, respectively, as shown in Figs. 2(a), (b), and (c). The simulation result is shown in Fig. 2(d) that the average torque and torque ripple of the three layers flux barriers where the ferrite material is embedded are better than that of one or two layers. Therefore, the rotor with ferrite-filled three-layer flux barriers is selected as the baseline structure of ERFa-SynRM, and the main design parameters are shown in Table 2.

3. OPTIMAL DESIGN OF MOTOR

Based on the preliminary design in the previous section, the topology of ERFa-SynRM will be optimally designed in this section, and the design process is divided into two steps. The first step is to design the overall dimensions of the motor, stator structure, and distributed winding parameters according to the conventional AC motor design line [16]. The second step is to design the motor's external rotor structure, flux barrier shape, and ,PM dimensions. As the torque ripple increases, the high

TABLE 2. ERFa-SynRM main design parameters.

Parameter	Unit	Value
Outer radius of stator	mm	170
Outer radius of rotor	mm	220
Stack length	mm	35
Rated voltage	V	48
Rated speed	r/min	350
Pole / slot	–	8/48
Number of turns	–	14
Air-gap length	mm	0.8

harmonics of the flux leakage will lead to higher iron losses and thus lower operating efficiency. Furthermore, the rotor temperature will also increase, resulting in the risk of the ferrite demagnetization. Hence, the distributed winding design strategy is used in the design of the motor. The stator structure of ERFa-SynRM is roughly the same as that of conventional AC motors, which will not be discussed in this paper. The focus here is on the optimal design of the external rotor structure.

The rotor structure is designed firstly to maximize the flux permeability of the d-axis and minimize the flux permeability of the q-axis in order to increase the ratio between the inductances based on formula (1). Then, multi-layer ferrite with low remanence density is added to the flux barrier in the direction of q-axis to improve the reluctance torque of the motor. According to formula (2), the electromagnetic torque is related to the number of phases, pole pairs, PM flux linkage, and input current [17]. The greater the salient pole ratio is, the higher the electromagnetic torque is. Moreover, the torque ripple T_{rip} is determined by the flux potential harmonics of stator f_{sh} and that of rotor f_{rh} based on formula (3), which are related to the air-gap permeability of the motor [18], implying that the reduction of the amplitude of the high harmonics can effectively suppress the torque ripple.

$$\xi = \frac{L_d}{L_q} \tag{1}$$

$$T_{em} = \frac{m}{2} \times \frac{p}{2} \times [\lambda_{pm}i_d + (L_d - L_q)i_d i_q] \tag{2}$$

$$T_{rip} = -\frac{p}{2}\frac{\mu_0}{g}r_g l\pi \sum_{\substack{h=6n\mp1 \\ n=1,2,3,\ldots}} (hf_{sh}f_{rh}\sin(h\pm1)\omega_e t\pm\gamma_d)) \tag{3}$$

where ξ is the salient pole ratio; L_q and L_d are the q-axis and d-axis inductances, respectively; T_{em} is the electromagnetic torque; λ_{pm} is the PM flux linkage; i_q and i_d are the q-axis and d-axis currents, respectively; g is the air-gap length; l is the stack length of the machine; μ_0 is the vacuum permeability; and γ_d is the phase angle of the current with the d-axis.

3.1. Optimization Objectives and Design Variables

The rotor flux barrier of ERFa-SynRM has a complex structure and diverse parameter matching, whose shape and dimension

have a large impact on the electromagnetic performance [19]. In this paper, 12 parameters that may have a strong correlation to the motor performance are selected as the design variables. Low torque ripple, high average torque, and high efficiency are selected as the optimization objectives of the motor. Different rotor geometries are generated by the optimization algorithm. The electromagnetic performances before and after the optimization are simulated and analyzed by the finite element analysis software to obtain the optimal motor design parameter that meets the design requirements, and all the selected design variables are shown in Fig. 3.
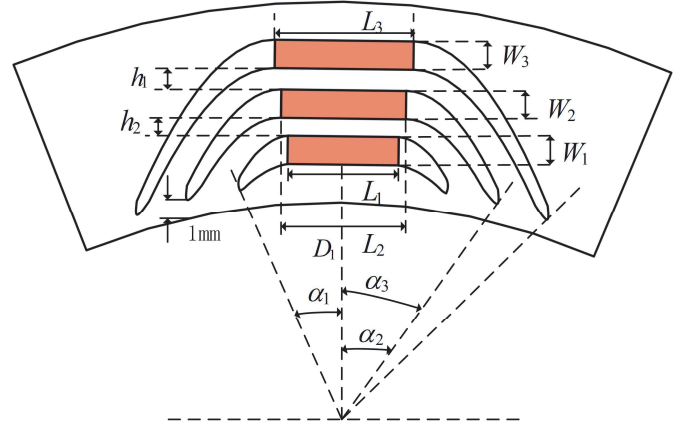
FIGURE 3. Model of geometrical parameters of ERFa-SynRM rotor.

In the multi-level optimization design process of the motor, the average torque, torque ripple, and efficiency are selected as the design objectives, and the objective function can be expressed as:

$$f(x_i)_{\min} = w_1\frac{T^*_{avg}(x_i)}{T_{avg}(x_i)} + w_2\frac{T^*_{rip}(x_i)}{T_{rip}(x_i)} + w_3\frac{\eta^*(x_i)}{\eta(x_i)}$$

$$\min x_i \leq x_i \leq \max x_i, \quad i = 1,2,3,\ldots,12 \tag{4}$$

where $T^*_{avg}(x_i)$, $T^*_{rip}(x_i)$, and $\eta^*(x_i)$ are the initial values of average torque, torque ripple, and efficiency, respectively. $T_{avg}(x_i)$, $T_{rip}(x_i)$, and $\eta(x_i)$ are the optimal values of average torque, torque ripple, and efficiency, respectively. x_i denotes the design variables. w_1, w_2, and w_3 are the weight coefficients of average torque, torque ripple, and efficiency, respectively, whose sum is 1. Generally, the choice of weighting coefficients has an important influence in the multi-level optimization process [20]. However, no single standard is given for determining the value of the weighting coefficient. In order to improve the stability and comfort of the motor during operation, the value of the torque ripple weighting coefficient w_2 is higher than the other two weighting coefficients and is set to 0.5. The weighting coefficients for the average torque w_1 and the efficiency w_3 are set to 0.25 and 0.25, respectively. Meanwhile, some constraints need to be obeyed during the optimization process, which are presented as follows:

$$T_{avg} \geq 7\,\text{N}\cdot\text{m}, \quad T_{rip} \leq 30\%, \quad \eta \geq 75\% \tag{5}$$

According to the 12 design variables selected above with high relevance, their sizes are rationalized, and the specific value ranges are shown in Table 3.

TABLE 3. Design variables and range of values.

Design Variable	Unit	Variation Ranges
L_1	mm	12–18
w_1	mm	3–4
α_1	deg	9–12
L_2	mm	14–22
w_2	mm	3–5
α_2	deg	13–17
L_3	mm	8–28
w_3	mm	3–5
α_3	deg	20–22
h_1	mm	2–4
h_2	mm	2–4
D_1	mm	88–91

3.2. Sensitivity Analysis

As can be seen from Table 3, the optimization of ERFa-SynRM topology is a multi-variable and strongly coupled nonlinear system optimization problem with a low degree of fit during the optimization process. In order to solve the problem of slow motor optimization due to the many design variables, a sensitivity analysis is performed to determine the strong and weak sensitive layers with different degrees of influence on the electromagnetic performance. The Pearson correlation coefficient can be expressed as follows:

$$\rho_{X_i, Y_i} = \frac{N \sum X_i Y_i - \sum X_i \sum Y_i}{\sqrt{N \sum X_i^2 - (\sum X_i)^2} \sqrt{N \sum Y_i^2 - (\sum Y_i)^2}} \quad (6)$$

where Y_i is the ith optimization objective, X_i the design variable, and N the number of samples.

According to formula (6), the Pearson correlation coefficients for different degrees of influence of the design variables on the optimization objective are calculated and shown in Fig. 4.

The design variables have different sensitivities to different optimization objectives. Combining (4) with (6), the value of the comprehensive sensitivity index $S_{com}(x_i)$ can be calculated through formula (7), and the results are shown in Fig. 5.

$$Scom(x_i) = w_1 \times |S_{Tavg}(x_i)| + w_2 \times |S_{Trip}(x_i)| + w_3 \times |S_\eta(x_i)| \quad (7)$$

where $S_{Tavg}(x_i)$, $S_{Trip}(x_i)$, and $S_\eta(x_i)$ are the Pearson correlation coefficients of the average torque, torque ripple, and efficiency with respect to the different design variables, respectively.

Weighing the optimized efficiency and calculated accuracy, the sensitivity threshold λ is set to 0.15 for judging the strong
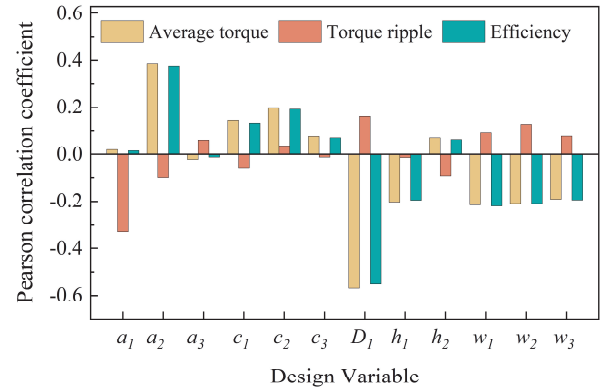
FIGURE 4. Pearson correlation coefficient.
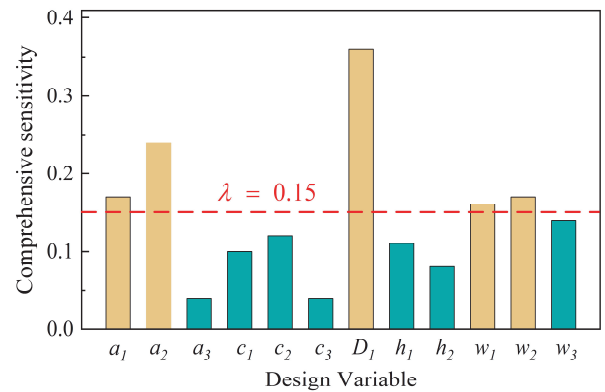
FIGURE 5. Comprehensive sensitivity index for the design variables.

and weak sensitivity stratification of the design variables. For the weak sensitive layer, the FEA software is used to simulate and analyze its electromagnetic performance, and the optimal simulation results are selected to determine the optimal size of the design variables. For the strong sensitive layer, the algorithm optimization is continued. The layering results are shown in Table 4.

TABLE 4. Stratification of the design variables.

Classification	Design variable
Sensitive	$D_1, \alpha_1, \alpha_2, w_1, w_2$
Insensitive	$\alpha_3, c_1, c_2, c_3, w_3$

4. MULTIOBJECTIVE OPTIMIZATION

Based on the strong sensitive layers identified in the previous section, the multi-objective optimization method of GA-BP combined with NSGA-II will be applied in this section to optimize the flux barrier structure of the rotor for ERFa-SynRM. For the different optimization objectives, a high-precision prediction model is constructed by GA-BP neural network. Following this, NSGA-II is used to perform global optimization search based on the prediction model to select the best design solution from the Pareto optimal set. The overall optimization process is shown in Fig. 6.

GA-BP predictive models

Determine the network structure

Preprocess imported data

Encode initial random weight values and thresholds

The training error as the fitness function

Selection, crossover, and mutation

Gen=Gen+1

Satisfaction of termination conditions? — N

Y

Decoding to obtain optimal weights and thresholds

Calculation error

Update weight values and thresholds

Satisfaction of termination conditions? — N

Y

Generating predictive models

NSGA-II optimization

Initializing NSGA-II parameters

Initialize the population Gen = 0

Initial population non-dominated ordering and crowding calculation

Bidding, selection of breeding parents

Bidding, selection of breeding parents

Crossover and mutation produce offspring, which merge with the parents to form a new population

After the non-dominated ordering and crowding calculation, the top N individuals in the population are taken

Gen=Gen+1

Gen≥Gen_Max? — N

Y

Exporting Pareto frontier solutions

Choose the optimal solution and verify it experimentally

FIGURE 6. Flowchart of multi-objective optimization design.

4.1. Constructing GABP Models

GA-BP neural network is a multi-layer feed-forward neural network that usually uses an input-implicit-output layer structure [21]. The design variables of the strong sensitive layer are used as the input values of the GA-BP algorithm, and the average torque, torque ripple, and efficiency are used as the out-put values of the GA-BP algorithm. The experimental sample data are obtained by the FEA software through which the design variables of the strong sensitive layer are scanned within the range of values. Among the 400 sets of the sample data, 350 sets are selected as the training set for the GA-BP algorithm, and 50 sets are selected as the test set for the GA-BP algorithm. The weights and thresholds of BP neural network
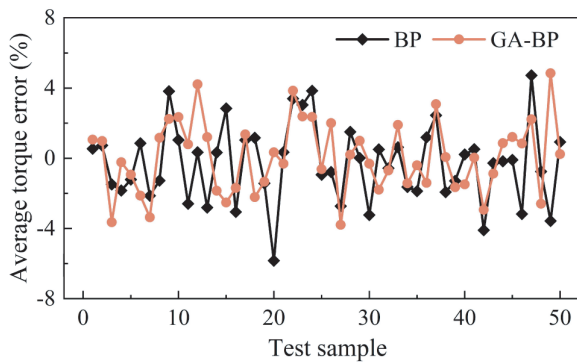
FIGURE 7. Average torque error.
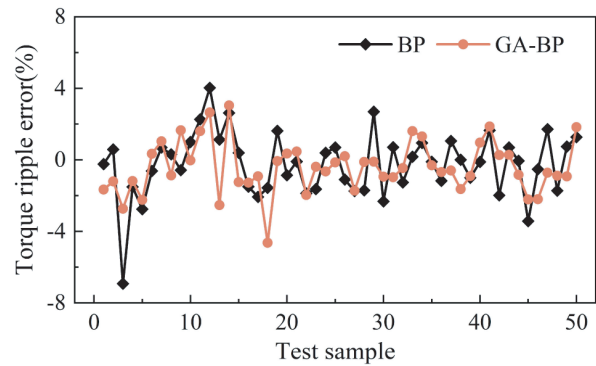
FIGURE 8. Torque ripple error.

TABLE 5. Comparison of the GA-BP and BP neural network prediction model error data.

Optimization objectives	GA-BP model error		BP model error	
	maximum error	average error	maximum error	average error
T_{avg}	4.8%	1.5%	5.8%	1.7%
T_{rig}	4.6%	1.1%	6.9%	1.4%
η	0.16%	0.05%	0.3%	0.06%

affect the prediction accuracy of the algorithm. If the values are not taken properly, the convergence speed of the algorithm will be affected, and it is easy to cause the weights and thresholds to fall into the local minimum. Here, GA is used to find the optimization of the weights and threshold variables of the BP to quickly obtain the optimal values and improve the prediction accuracy of the prediction model. After training and testing, the results of the optimal fitting error for average torque, torque ripple, and efficiency are shown below.

From the error diagrams in Figs. 7, 8, and 9, it can be seen that compared with the conventional BP neural network prediction model, the training error obtained by using the GABP algorithm is lower. The specific error comparison data are shown in Table 5.
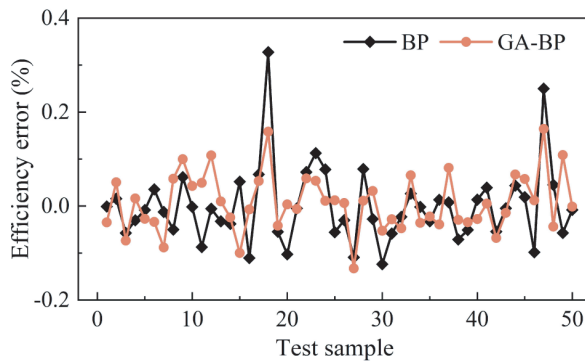
FIGURE 9. Efficiency error.

4.2. Optimization Based on NSGA-II

The NSGA-II is a multi-objective optimization algorithm based on non-dominated relations proposed by Deb et al. [22]. The algorithm incorporates a tournament mechanism and an elite

retention strategy, which enhance the global search ability of the algorithm, reduces the complexity, accelerates the convergence, and shortens the computational time of the motor performance optimization. The optimal prediction model of the GA-BP method is used as the optimization function of the NSGA-II algorithm. By adjusting the main parameters of the NSGA-II algorithm, such as setting the number of population iterations to 50, the number of populations to 30, and the crossover and variance values to 0.9 and 0.1, respectively, the optimization algorithm is run to obtain the optimal set of solutions for the Pareto front, and the results are shown in Fig. 10.

The Pareto front refers to the optimal solution set in which all the solutions are not dominant over each other. The main goal of the optimization design in this paper is to reduce the torque ripple of the motor. When the average torque and efficiency performance of the motor meet certain requirements, the red five-pointed star in Fig. 10 is taken as the optimal value of the
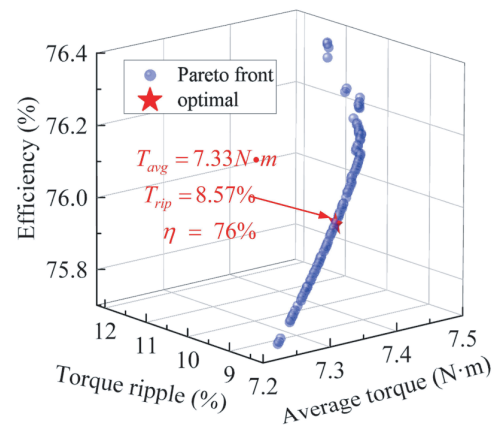
FIGURE 10. Pareto front.
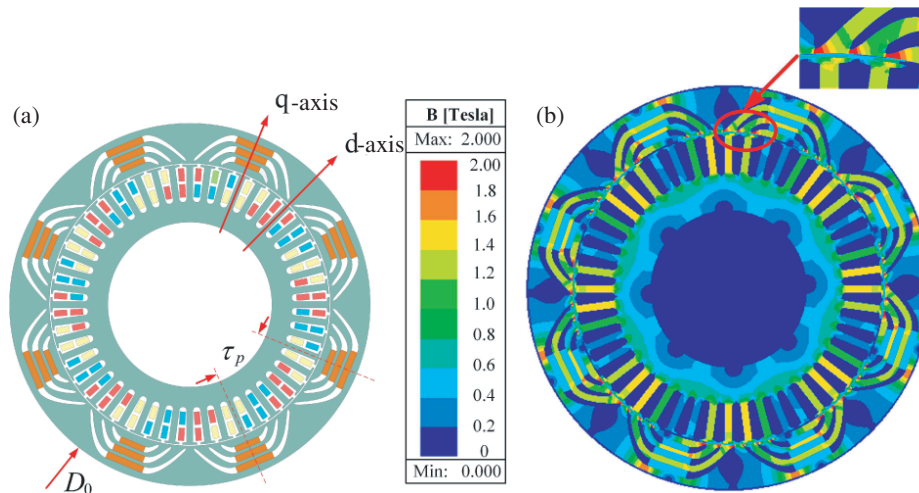
FIGURE 11. Final topology of ERFa-SynRM. (a) Top view of d-q axis and pole distance. (b) Flux density.

torque ripple. Meanwhile, the average torque and efficiency are at the median level, which meets the design requirements of the motor.

The parameter values and performance comparison between the optimal and initial designs of the motor are shown in Table 6. From Table 6, it can be seen that the design scheme optimized by the multi-objective strategy meets the requirements of the optimization objectives and constraints, thus obtaining the optimal performance topology structure of ERFa-SynRM.

TABLE 6. Comparison of main parameters before and after optimization.

Design variables	Unit	Initial value	Optimal value
L_1	mm	16	15.13
w_1	mm	4	3.51
α_1	deg	10	10.8
L_2	mm	18	20.93
w_2	mm	4	4
α_2	deg	15	15.82
L_3	mm	20	21.85
w_3	mm	4	4.36
α_3	deg	20	20.84
h_1	mm	2.5	2.01
h_2	mm	3	3.29
$D1$	mm	89	89.6
T_{avg}	N·m	7.14	7.33
T_{rip}	%	19	8.57
η	%	75	76

5. COMPARISON OF MOTOR PERFORMANCE

The optimized motor structure is shown in Fig. 11(a). In order to verify the effectiveness of the optimization strategy, this section further analyzes and evaluates the electromagnetic performances of the optimal topology obtained by the multi-objective optimization. The FEA software is used to simulate and analyze the performance of the initial design motor and the optimized motor in terms of the inductance characteristics, air-gap flux density, torque characteristics, and back electromotive force (EMF). Fig. 11(b) shows the flux density of the motor under the operating conditions of rated current of 10 A, rated power of 265 W, and rated speed of 350 r/min, which demonstrates that the core saturation distribution of the optimized motor means better, and the highest flux density is located at the end of the rotor flux barrier. The flux density reaches up to 2 T, which can effectively reduce the motor's flux leakage and lower the impact on the average torque performance.

5.1. No-Load Characteristics

In order to verify the structural design of ERFa-SynRM, no-load characteristics of the motor are simulated and analyzed at rated speed of 350 r/min.

The airgap flux density reflects the motor torque output capability, which has a certain influence on the torque performance, vibration, and noise generation. Fig. 12 shows the results of the analysis of the flux density waveform and harmonic content before and after optimization. The optimized airgap flux density waveform of the motor is more symmetrical than that of the pre-optimization one. The flux density amplitude increases from 0.114 T before optimization to 0.127 T after optimization. Compared with the initial motor, the 3rd harmonic and 7th harmonic amplitudes are lower after optimization, which means that the optimization has a better suppression of torque ripple.

The back EMF is induced by the armature windings cutting the flux field. The better the sinusoidality is and the higher the amplitude is, the more conducive is to improve the torque output capacity. Fig. 13 gives the waveform and harmonic content results of the no-load back EMF of the motor before and after optimization. As shown in Fig. 13(a), the optimized no-load back EMF waveform is closer to a sinusoidal waveform. As shown in Fig. 13(b), the fundamental frequency harmonic amplitude of the initial motor is 5.16 V, and the fundamental frequency harmonic amplitude of the optimized motor is 5.76 V. The fundamental frequency amplitude of the optimized motor
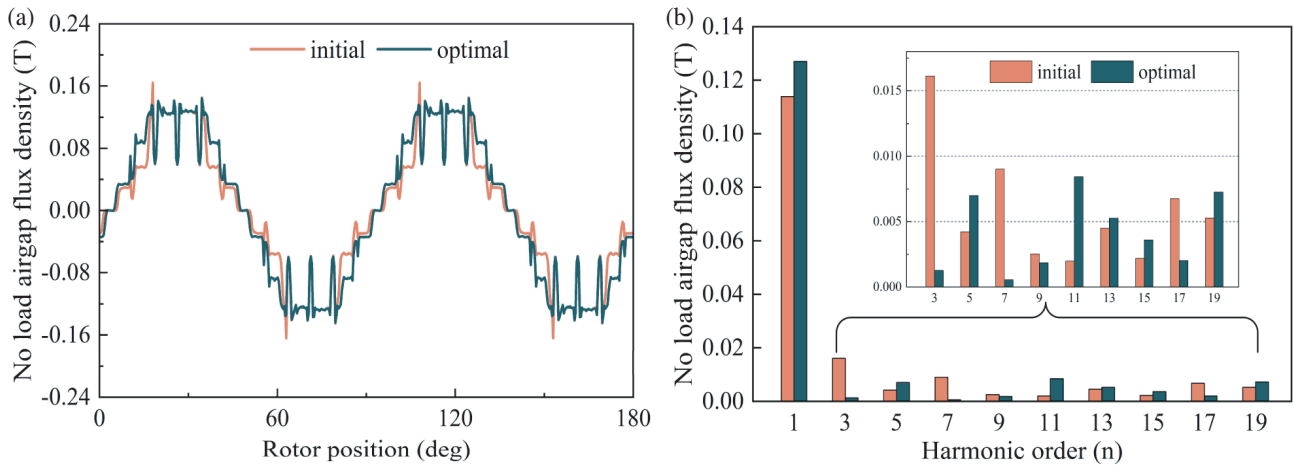
FIGURE 12. Comparison of air gap flux density before and after optimization. (a) Waveforms. (b) Harmonic.
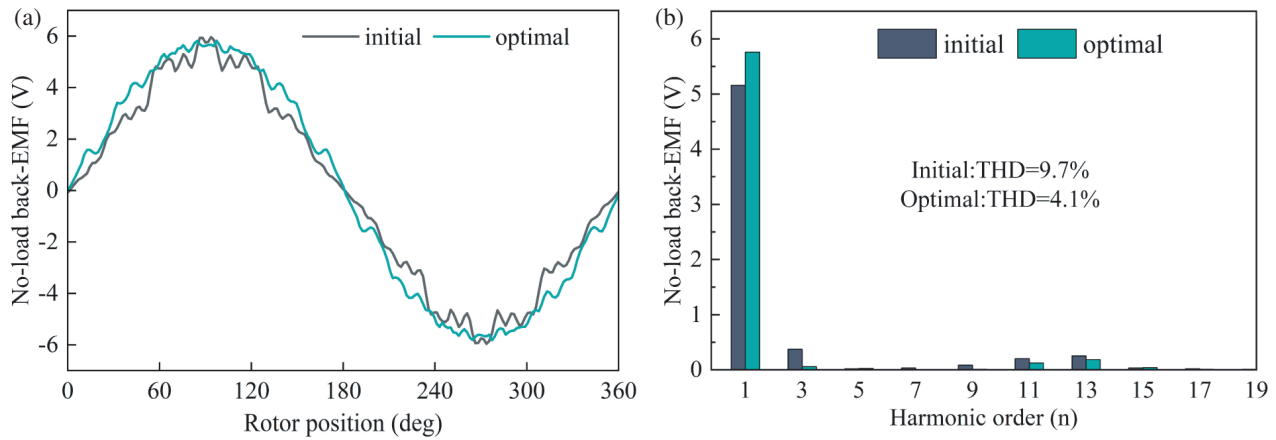
FIGURE 13. Comparison of no-load back EMF before and after optimization. (a) Waveforms. (b) Harmonic.
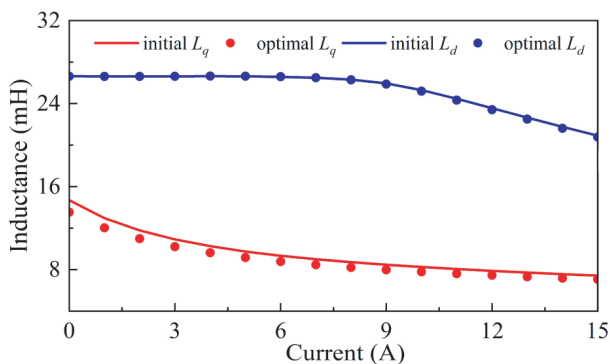
FIGURE 14. d-q axis inductance before and after optimization.
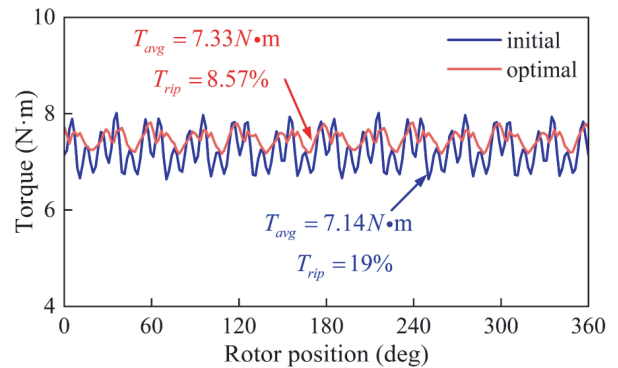
FIGURE 15. Comparison of torque curves before and after optimization.

is 11.6% higher than that of the initial motor, and the high harmonic content is significantly reduced. The total harmonic distortion rate of the initial motor is 9.7%, and the total harmonic distortion rate of the optimized motor is 4.1%, which is reduced by 57.2%. Compared with the initial motor, the sinusoidal characterization of the no-load back EMF waveform of the optimized motor is improved.

5.2. Torque Characteristic

From formula (2), the electromagnetic torque T_{em} is proportional to the inductance difference ($L_d L_q$), so the average torque of the motor can be increased by improving the salient pole ratio. The performance output curves of the motor before and after optimization at the rated operating conditions are given in Fig. 14 and Fig. 15. From Fig. 14, it can be seen that the

inductance characteristic of the d-q axis is improved; the salient pole ratio before optimization is 3.07; and after optimization, the salient pole ratio is increased to 3.24. From Fig. 15, it can be seen that the average torque before optimization is $7.14\,\mathrm{N \cdot m}$, and after optimization, it is $7.33\,\mathrm{N \cdot m}$, which is a slight increase in the average torque. After optimization, the torque ripple is reduced from 19% to 8.57%. From the above comparison of the motor performance, it can be seen that the improvement of the inductance characteristics plays an important role in increasing the average torque and reducing the torque ripple of the motor.

6. CONCLUSION

GA-BP-NSGA-II multi-objective optimization design method is proposed for the ERFa-SynSRM in this paper. The optimization process includes the sensitivity analysis, GA-BP prediction model, and optimization of the NSGA-II algorithm. The electromagnetic performances of the motor before and after optimization are compared by using the FEA software. The results show that although the efficiency and average torque of the optimized motor do not change much, the optimization effect of suppressing torque ripple is obvious, which decreases from 19% before optimization to 8.57% after optimization, a reduction of 54.9%. The effectiveness of the multi-objective optimization algorithm is verified.

ACKNOWLEDGEMENT

REFERENCES

[1] Nicorici, A.-M., C. Oprea, and C. Martis, "Performance evaluation of a 7.5 kW permanent magnet assisted synchronous reluctance machine for light electric vehicles," in *2018 International Conference and Exposition on Electrical And Power Engineering (EPE)*, 0129–0132, Iasi, Romania, 2018.

[2] Peng, C., D. Wang, Z. Feng, and B. Wang, "A new segmented rotor to mitigate torque ripple and electromagnetic vibration of interior permanent magnet machine," *IEEE Transactions on Industrial Electronics*, Vol. 69, No. 2, 1367–1377, 2021.

[3] Di, C., X. H. Bao, J. Pan, and C. Y. Wang, "Modelling and analysis of a ferrite assisted synchronous reluctance machine based on the open-source platform elmer," *Transactions of China Electrotechnical Society*, Vol. 37, No. 5, 1136–1144, 2022.

[4] Zhang, Q.-Z., L.-B. Niu, and Y.-L. Ai, "Performance analysis of permanent magnet assisted reluctance synchronous machine," *Power System Protection and Control*, Vol. 39, No. 22, 129–132, 2011.

[5] Jin, W., L. Yan, J. Jianguo, J. Yongteng, and Z. Jialin, "Analysis of the influence of back-EMF and saliency ratio on steadystate characteristics of a high efficiency permanent magnet synchronous reluctance motor," *Transactions of China Electrotechnical Society*, Vol. 35, No. 22, 4688–4698, 2020.

[6] Yan, D., Y. Dong, J. Kai, and G. Jin, "Rotor optimal design of the gradient flux-barrier for torque ripple reduction in synchronous reluctance motor," *Transactions of China Electrotechnical Soci-*

[7] Liu, R., D. Yan, and L. Jing, "Astroid rotor structural design and analysis of a synchronous reluctance motor," *Electric Machines and Control*, Vol. 26, No. 10, 49–55, 2022.

[8] Bonthu, S. S. R., M. T. B. Tarek, and S. Choi, "Optimal torque ripple reduction technique for outer rotor permanent magnet synchronous reluctance motors," *IEEE Transactions on Energy Conversion*, Vol. 33, No. 3, 1184–1192, 2017.

[9] Deshpande, Y. and H. A. Toliyat, "Design of an outer rotor ferrite assisted synchronous reluctance machine (Fa-SynRM) for electric two wheeler application," in *2014 IEEE Energy Conversion Congress and Exposition (ECCE)*, 3147–3154, Pittsburgh, PA, USA, 2014.

[10] Bonthu, S. S. R., S. Choi, and J. Baek, "Design optimization with multiphysics analysis on external rotor permanent magnet-assisted synchronous reluctance motors," *IEEE Transactions on Energy Conversion*, Vol. 33, No. 1, 290–298, 2017.

[11] Mohammed, M. S. and R. A. Vural, "NSGA-II+ FEM based loss optimization of three-phase transformer," *IEEE Transactions on Industrial Electronics*, Vol. 66, No. 9, 7417–7425, 2018.

[12] Hua, Y., H. Zhu, and Y. Xu, "Multi-objective optimization design of bearingless permanent magnet synchronous generator," *IEEE Transactions on Applied Superconductivity*, Vol. 30, No. 4, 1–5, 2020.

[13] Huang, C., H. Yuan, and Y. Geng, "Multi-objective optimization method for permanent magnet-assisted switched reluctance motor with GASVM-NSGA-II[J/OL]," Mechanical Science and Technology for Aerospace Engineering, 1–8.

[14] Kwon, M.-S. and D.-K. Lim, "A study on the optimal design of PMa-SynRM for electric vehicles combining random forest and genetic algorithm," *IEEE Access*, Vol. 11, 52 357–52 369, 2023.

[15] Bozkurt, A., A. F. Baba, and Y. Oner, "Design of outer-rotor permanent-magnet-assisted synchronous reluctance motor for electric vehicles," *Energies*, Vol. 14, No. 13, 3739, 2021.

[16] Pellegrino, G., T. M. Jahns, N. Bianchi, W. L. Soong, and F. Cupertino, "The rediscovery of synchronous reluctance and ferrite permanent magnet motors: Tutorial course notes," 2016.

[17] Zhu, J., K. W. E. Cheng, and X. Xue, "Torque analysis for in-wheel switched reluctance motors with varied number of rotor poles," in *2016 International Symposium on Electrical Engineering (ISEE)*, 1–5, Hong Kong, China, 2016.

[18] Baek, J., S. S. R. Bonthu, and S. Choi, "Design of five-phase permanent magnet assisted synchronous reluctance motor for low output torque ripple applications," *IET Electric Power Applications*, Vol. 10, No. 5, 339–346, 2016.

[19] Bacco, G., N. Bianchi, and H. Mahmoud, "A nonlinear analytical model for the rapid prediction of the torque of synchronous reluctance machines," *IEEE Transactions on Energy Conversion*, Vol. 33, No. 3, 1539–1546, 2018.

[20] Zhao, W., A. Ma, J. Ji, X. Chen, and T. Yao, "Multiobjective optimization of a double-side linear vernier PM motor using response surface method and differential evolution," *IEEE Transactions on Industrial Electronics*, Vol. 67, No. 1, 80–90, 2019.

[21] Han, S.-H., T. M. Jahns, W. L. Soong, M. K. Güven, and M. S. Illindala, "Torque ripple reduction in interior permanent magnet synchronous machines using stators with odd number of slots per pole pair," *IEEE Transactions on Energy Conversion*, Vol. 25, No. 1, 118–127, 2010.

[22] Deb, K., A. Pratap, S. Agarwal, and T. Meyarivan, "A fast and elitist multiobjective genetic algorithm: NSGA-II," *IEEE Transactions on Evolutionary Computation*, Vol. 6, No. 2, 182–197, 2002.